Supplementary material for LHCb-PAPER-2021-023

This appendix contains supplementary material that will be posted on the public CDS record but will not appear in the paper.

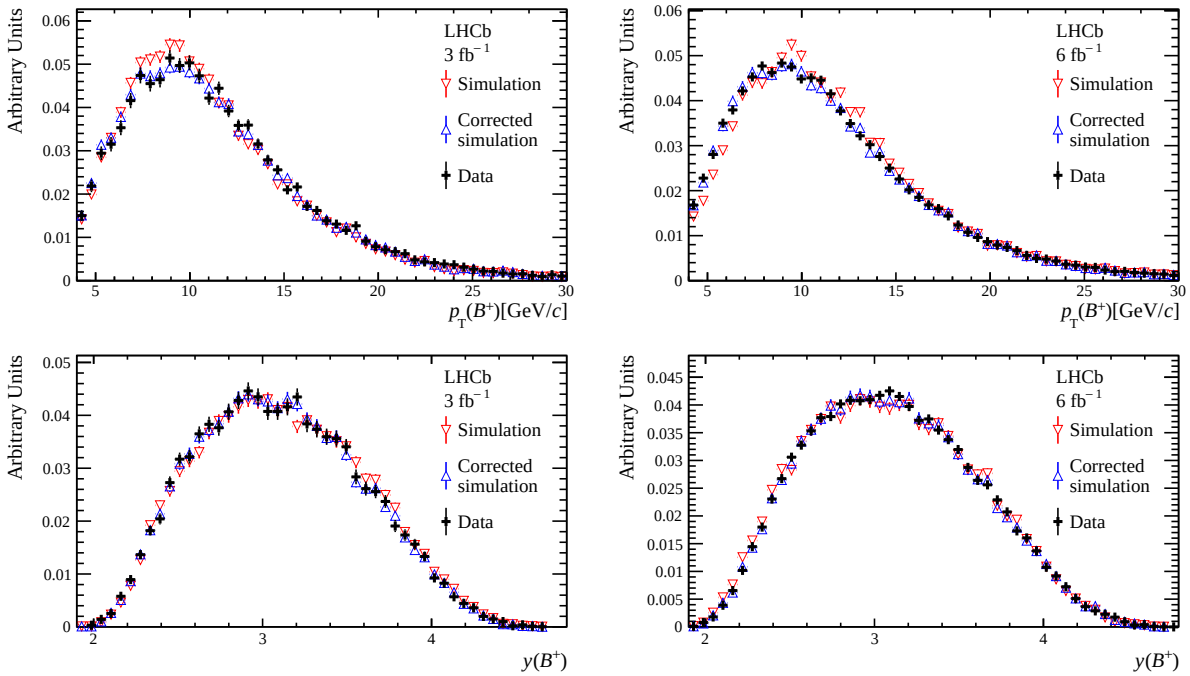

Figure S1: Kinematic distributions of $B^+ \to D_s^+ \overline{D}^0$ decays, compared between data and simulation before and after kinematic corrections. Distributions are shown relative to (top) transverse momentum and (bottom) rapidity, for (left) Run 1 data and (right) Run 2 data.

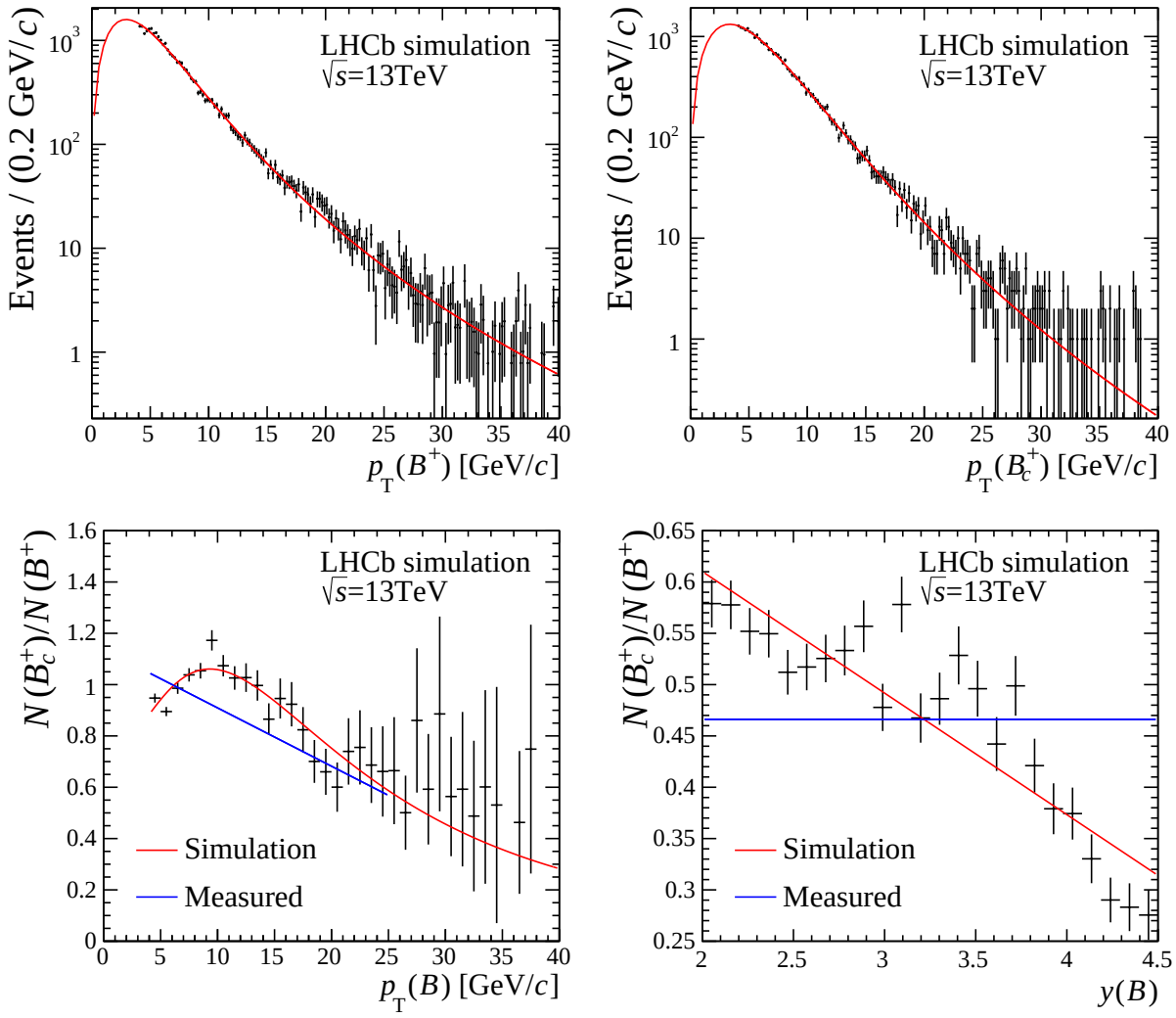

Figure S2: Simulated production spectra in p_{T} of (left top) B_c^+ from BCVEGPY and (right top) B^+ from PYTHIA with fitted Tsallis functions overlaid. Ratio of B_c^+ to B^+ simulated production spectra in (bottom left) p_{T} and (bottom right) y with the fitted function (red) and measured ratio (blue) overlaid.

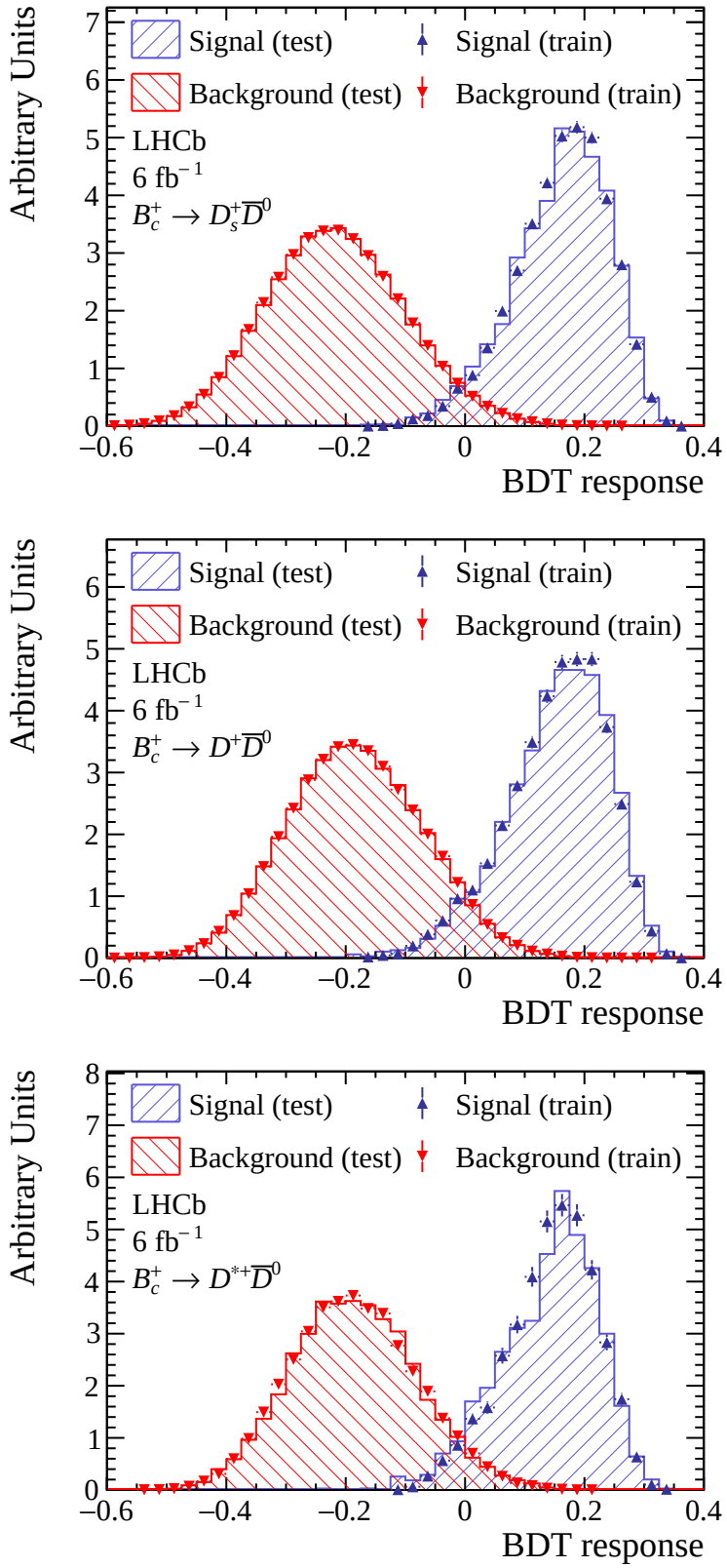

Figure S3: Comparison of the BDT response to simulated B_c^+ signal and background B candidates from the data sideband region. The plots correspond to (first row) $B_c^+ \to D_s^+ \overline{D}^0$ decays, (second row) $B_c^+ \to D^+ \overline{D}^0$ decays and (third row) $B_c^+ \to D^{*+} \overline{D}^0$ decays with $D^0 \to K^- \pi^+$ in Run 2 data. These plots demonstrate the performance of the BDT in separating background from signal.

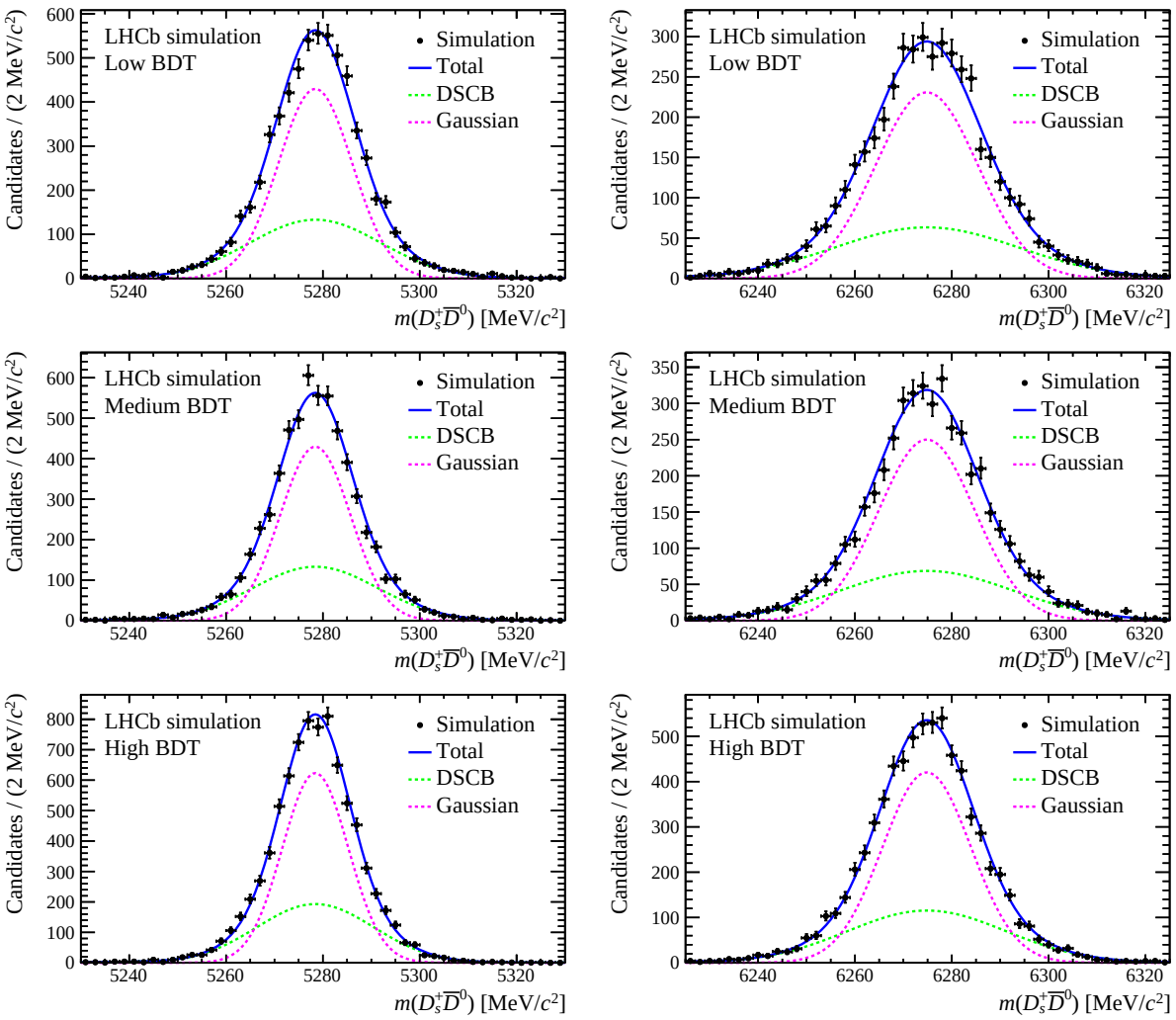

Figure S4: Distributions of the reconstructed mass of simulated (left) $B^+ \to D_s^+ \overline{D}^0$ and (right) $B_c^+ \to D_s^+ \overline{D}^0$ decays for the (top) lowest, (middle) intermediate, and (bottom) highest BDT samples. The overlaid fit corresponds to a narrow Gaussian and a wider double-sided Crystal Ball function. Note that the overall width differs between BDT samples.

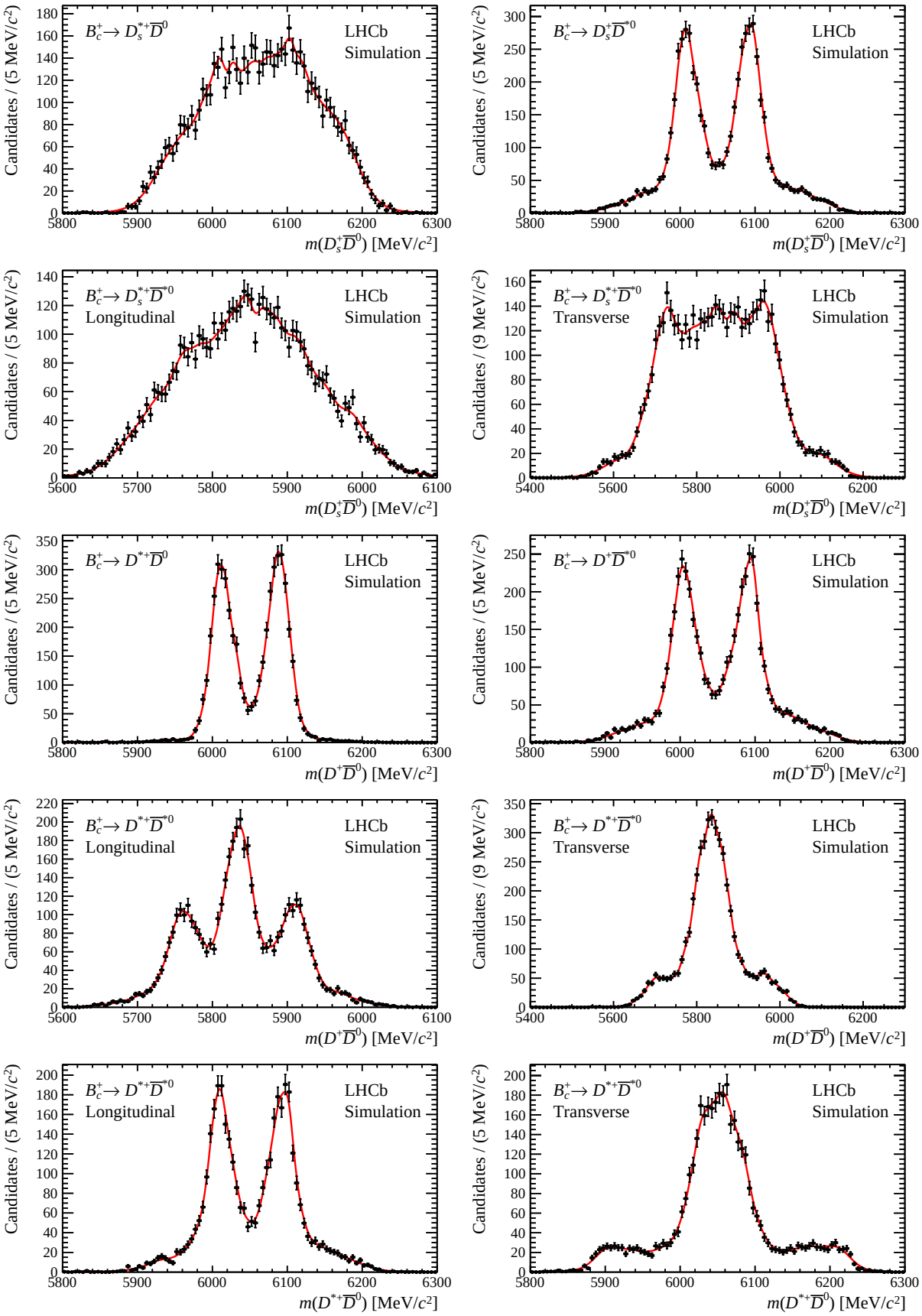

Figure S5: Distributions of the reconstructed mass of simulated (first row) $B_c^+ \to D_s^{(*)+}\overline{D}^{(*)0}$ decays with one missing particle, (second row) $B_c^+ \to D_s^{*+}\overline{D}^{*0}$ decays with two missing particles, (third row) $B_c^+ \to D^{(*)+}\overline{D}^{(*)0}$ decays with one missing soft particle, (second row) $B_c^+ \to D^{*+}\overline{D}^{*0}$ decays with two missing particles and (fifth row) $B_c^+ \to D^{*+}\overline{D}^{*0}$ decays with one missing particle. A kernel density estimator is overlaid.

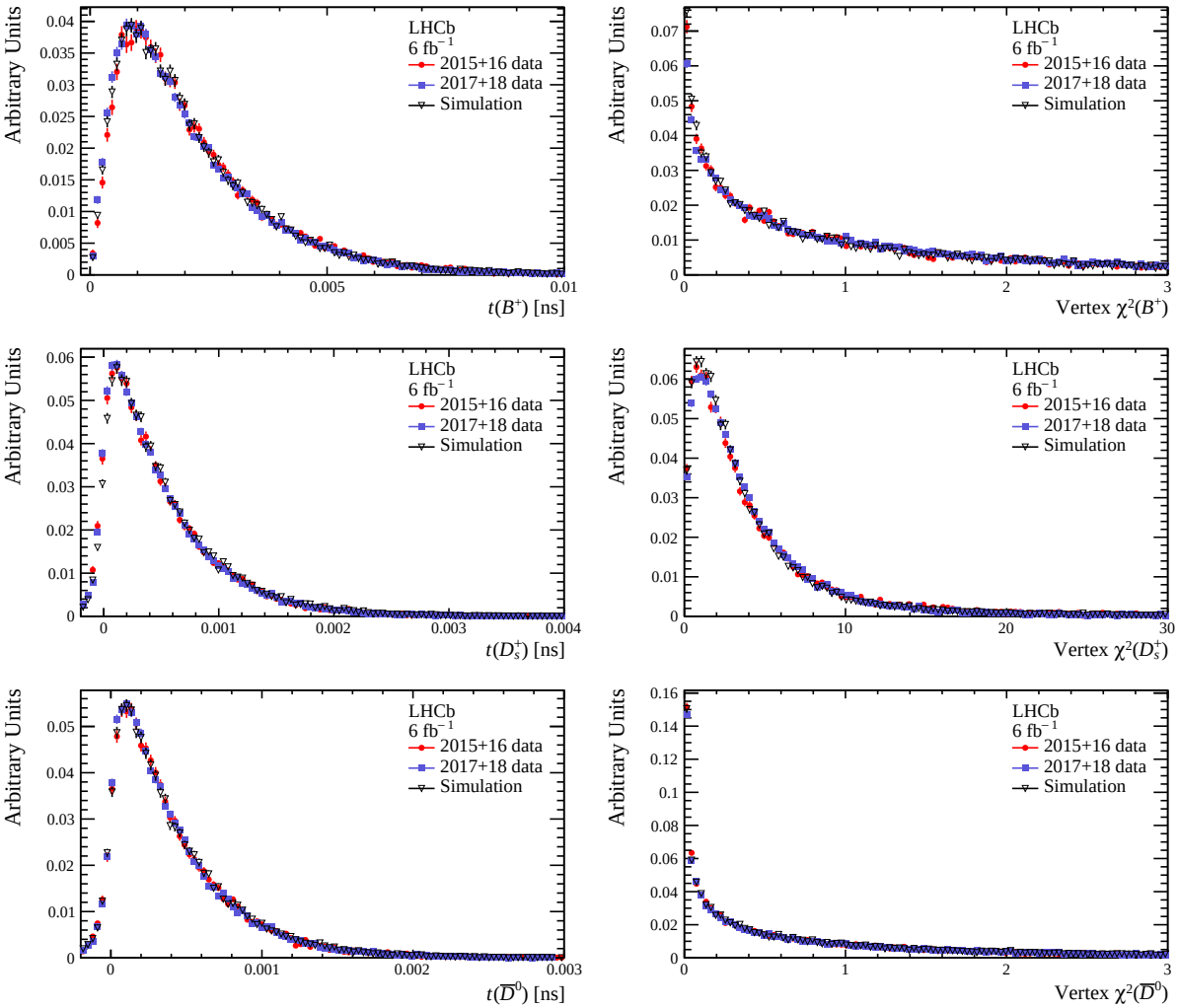

Figure S6: Comparison between Run 2 data and simulation of $B^+ \to D_s^+ \overline{D}^0$ decays for distributions of (top left) the B^+ proper lifetime, (top right) the B^+ vertex χ^2, (middle left) the D_s^+ proper lifetime, (middle right) the D_s^+ vertex χ^2, (bottom left) the D_s^+ proper lifetime, and (bottom right) the D^0 vertex χ^2. For the data distributions, background has been subtracted using the B^+ mass sidebands.

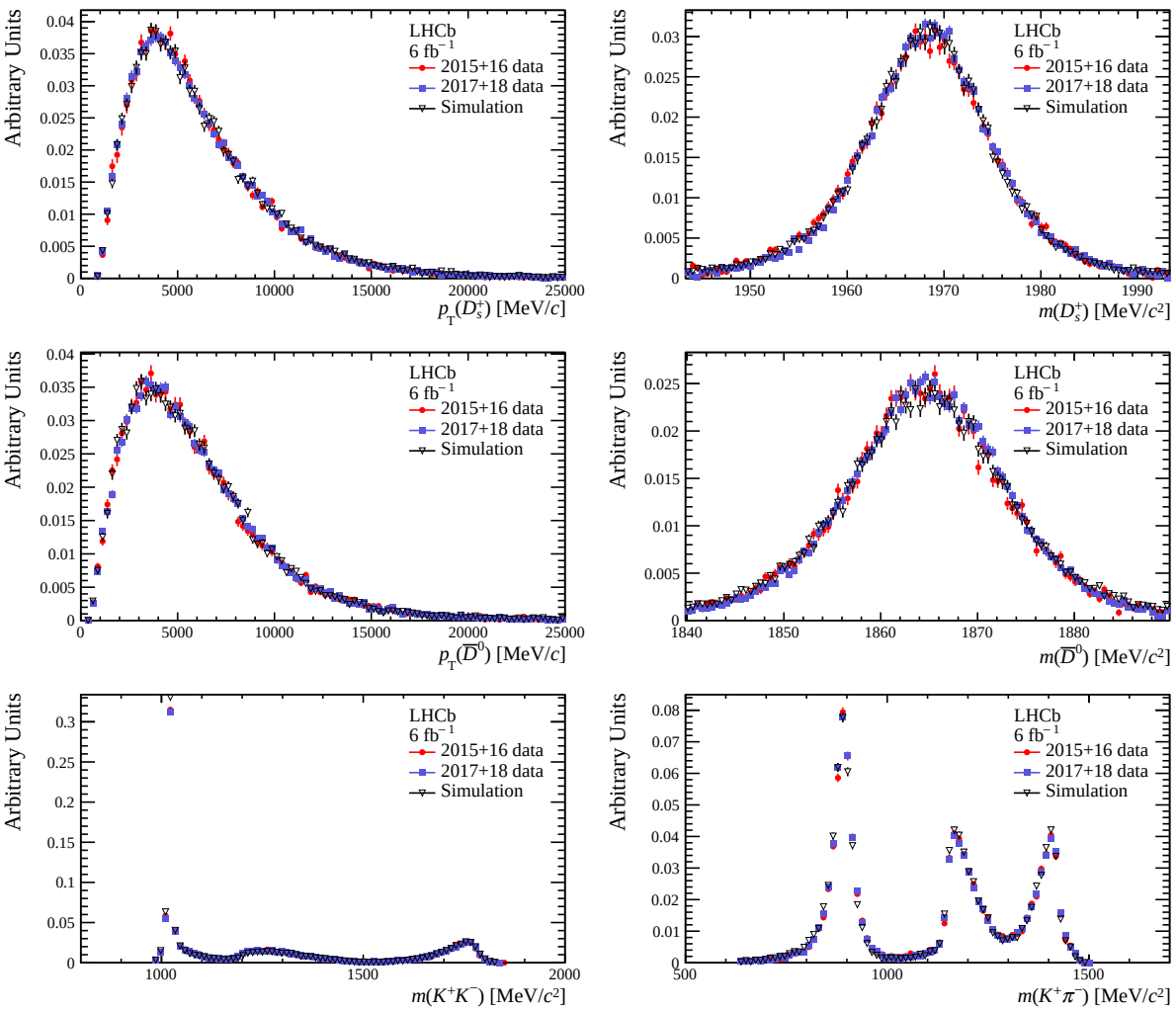

Figure S7: Comparison between Run 2 data and simulation of $B^+ \to D_s^+ \overline{D}^0$ decays for distributions of (top left) the D_s^+ transverse momentum, (top right) the D_s^+ invariant mass, (middle left) the D^0 transverse momentum, (middle right) the D^0 invariant mass, (bottom left) the K^+K^- invariant mass, and (bottom right) the $K^-\pi^+$ invariant mass. For the data distributions, background has been subtracted using the B^+ mass sidebands.

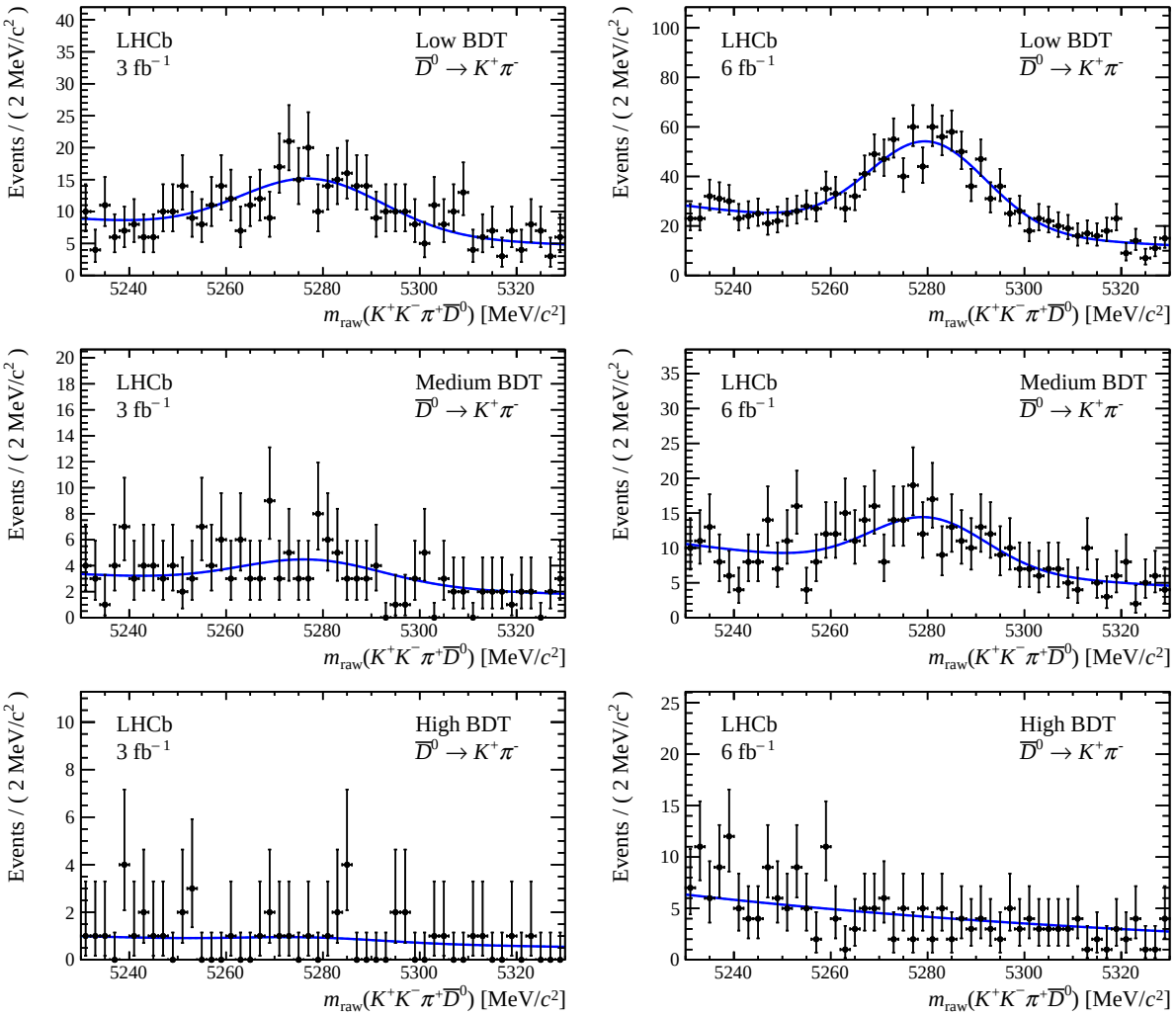

Figure S8: Distributions of the raw B mass from the D_s^+ sidebands of $B^+ \to D_s^+\overline{D}^0$ candidates in (left) Run 1 and (right) Run 2 data, for the (top) lowest, (middle) intermediate, and (bottom) highest BDT samples. The overlaid fit corresponds to an exponential for the combinatorial background plus a Gaussian for the signal. The fit is applied simultaneously to the three BDT samples, with a common shape and position of the Gaussian function. The results of these fits are used to determine the yield of $B^+ \to \overline{D}^0 K^+K^-\pi^+$, which is a background to the $B^+ \to D_s^+\overline{D}^0$ normalisation channel with less than 1% of its yield.

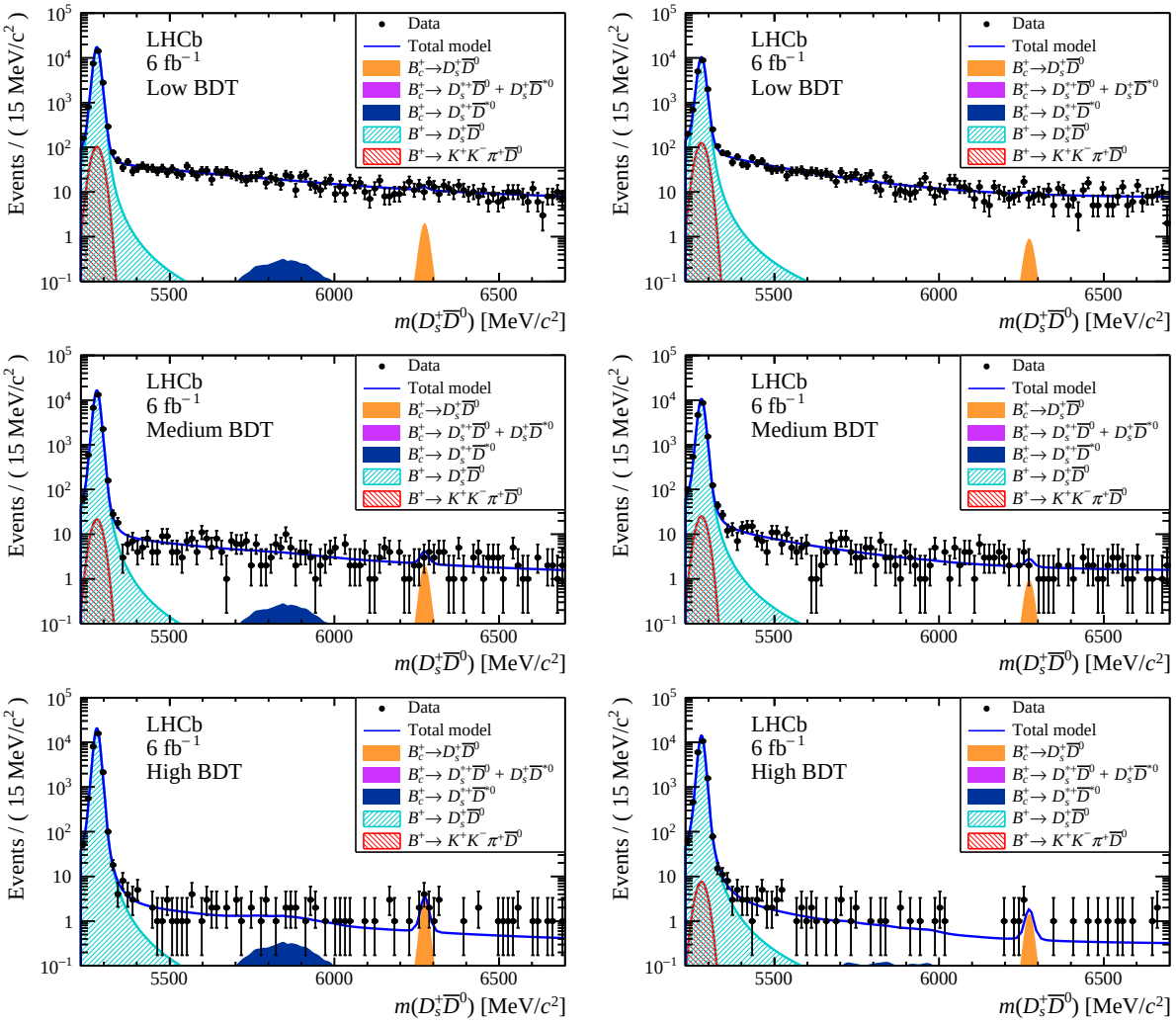

Figure S9: Selected $B^+_{(c)} \to D_s^+ \overline{D}^0$ candidates with (left) $D^0 \to K^-\pi^+$ and (right) $D^0 \to K^-\pi^+\pi^-\pi^+$ for data corresponding to the (top) lowest, (middle) intermediate, and (bottom) highest BDT sample, for Run 2 data. The overlaid curve represents a fit that is common for all six plots. These plots demonstrate how all BDT samples and D^0 decay channels are combined into a single combined fit. The highest BDT sample has the lowest background and provides most of the sensitivity to the B_c^+ signal, while the lower BDT samples increase the signal efficiency and help constrain the shape of the combinatorial background.

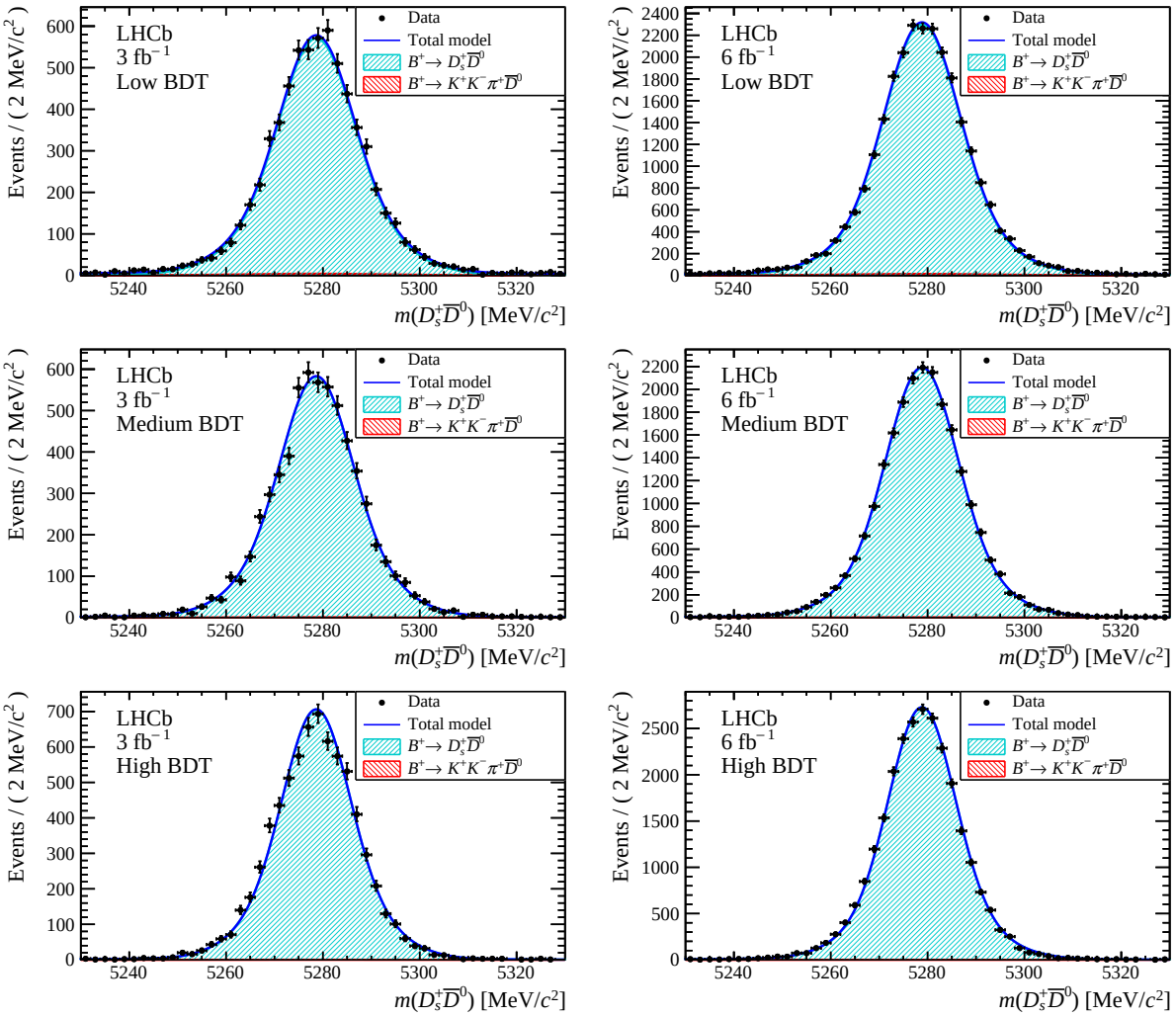

Figure S10: Selected $B^+_{(c)} \to D^+_s \overline{D}^0$ candidates, with $D^0 \to K^-\pi^+$, for masses near $m(B^+)$, for data corresponding to the (top) lowest, (middle) intermediate, and (bottom) highest BDT sample, for (left) Run 1 data and (right) Run 2 data. These plots demonstrate the small backgrounds in all BDT samples and the description of the data by the B^+ signal model, including the BDT-dependence of the mass resolution. Note that the B^+ signals are well contained within the fit range starting at 5230 MeV/c^2.

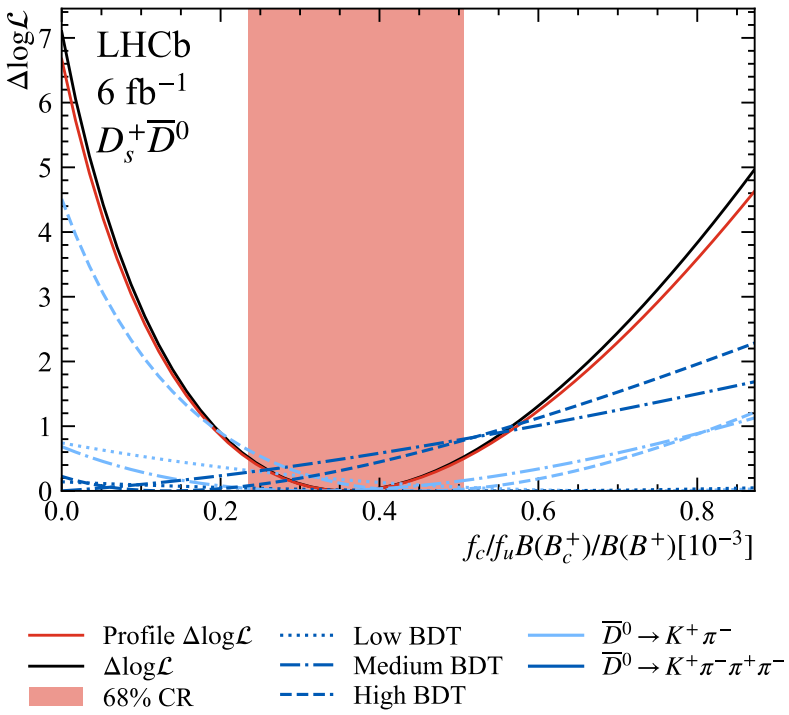

Figure S11: The (black) delta log likelihood and (red) profile likelihood for $B_c^+ \to D_s^+ \overline{D}^0$ decays in Run 2 data, including (blue) delta log profile likelihoods from individual final states and BDT samples. The 68% confidence interval is shaded.

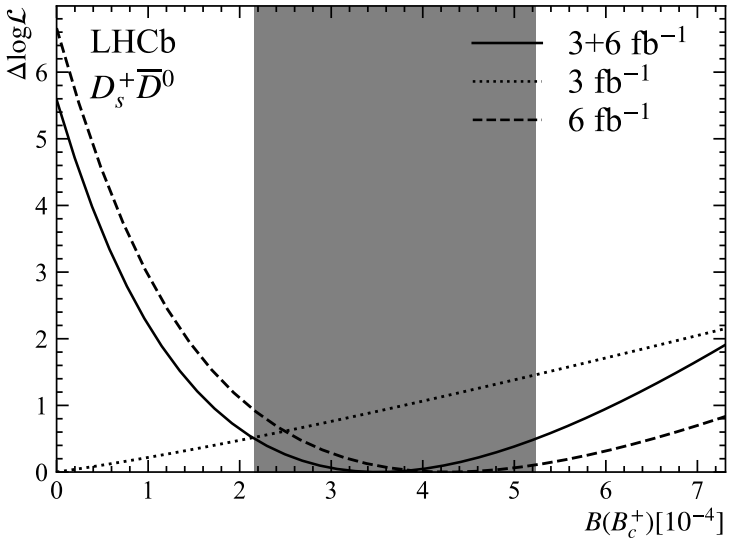

Figure S12: Delta log profile likelihood in (dotted line) Run 1 data, (dashed line) Run 2 data and (solid line) Run 1+2 data for $B_c^+ \to D_s^+ \overline{D}^0$ decays. The 68% confidence interval is shaded.

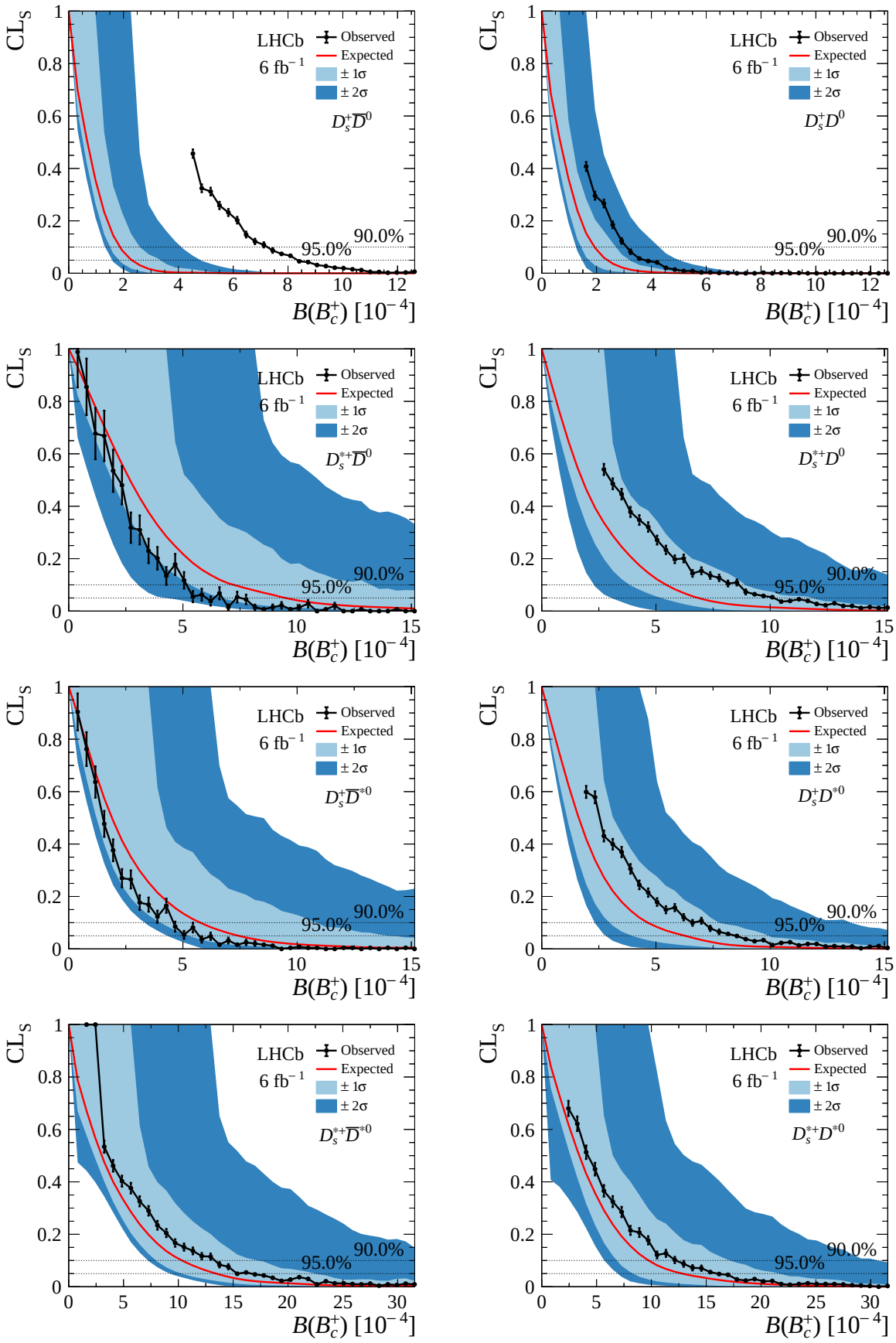

Figure S13: CL$_s$ distributions for the branching fractions of (first row left) $B_c^+ \to D_s^+ \overline{D}^0$, (first row right) $B_c^+ \to D_s^+ D^0$, (second row left) $B_c^+ \to D_s^{*+} \overline{D}^0$, (second row right) $B_c^+ \to D_s^{*+} D^0$, (third row left) $B_c^+ \to D_s^+ \overline{D}^{*0}$, (third row right) $B_c^+ \to D_s^+ D^{*0}$, (fourth row left) $B_c^+ \to D_s^{*+} \overline{D}^{*0}$, and (fourth row right) $B_c^+ \to D_s^{*+} D^{*0}$ decays in Run 2 data.

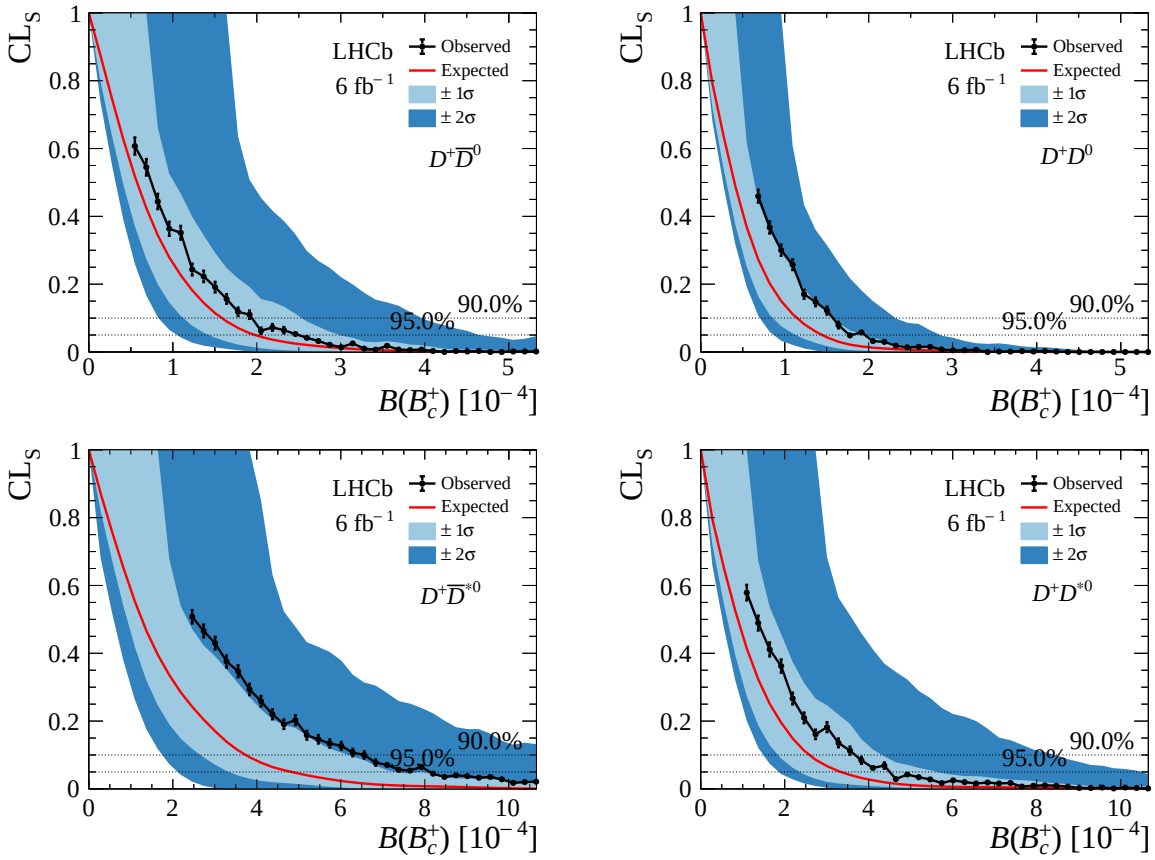

Figure S14: CL$_s$ distributions for the branching fractions of (top left) $B_c^+ \to D^+\overline{D}^0$, (top right) $B_c^+ \to D^+D^0$, (bottom left) $B_c^+ \to D^+\overline{D}^{*0}$, and (bottom right) $B_c^+ \to D^+D^{*0}$ decays in Run 2 data.

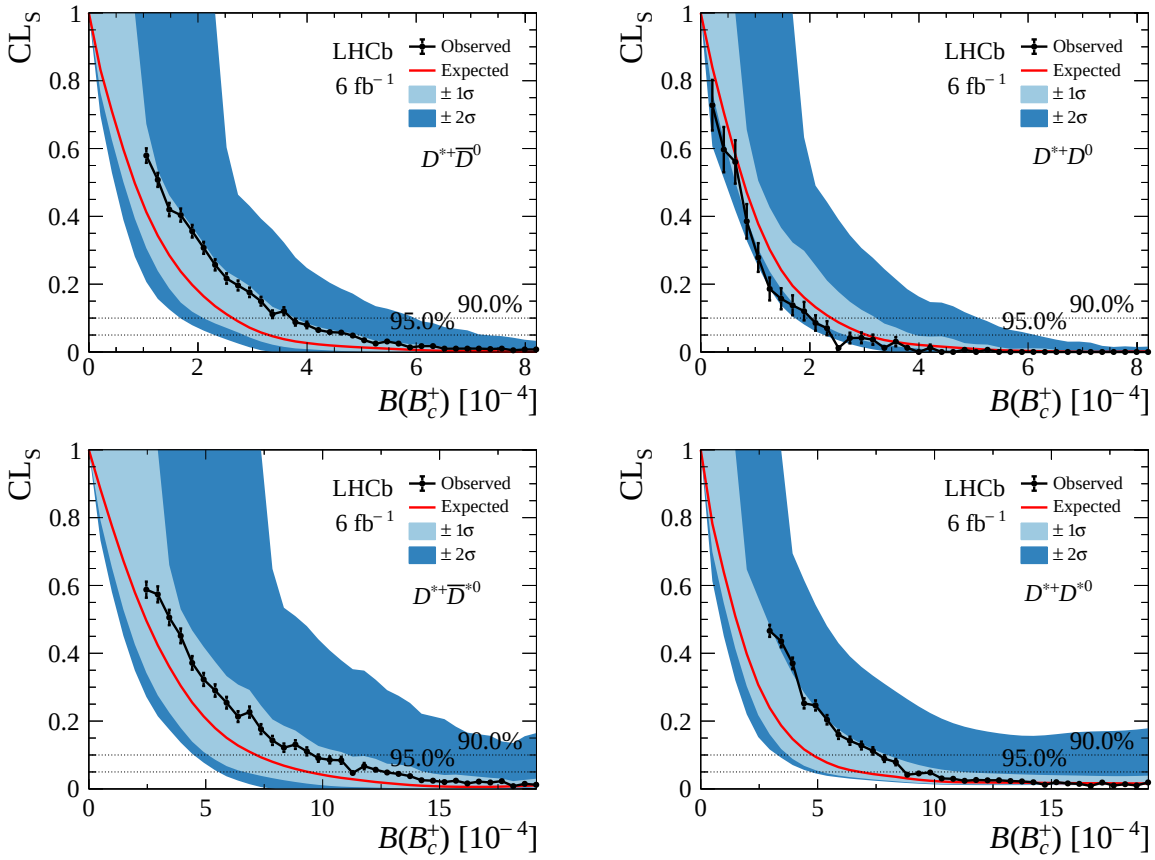

Figure S15: CL$_s$ distributions for the branching fractions of (top left) $B_c^+ \to D^{*+}\overline{D}^0$, (top right) $B_c^+ \to D^{*+}D^0$, (bottom left) $B_c^+ \to D^{*+}\overline{D}^{*0}$, and (bottom right) $B_c^+ \to D^{*+}D^{*0}$ decays in Run 2 data.